ON THE STABILIZING INFLUENCE OF SILT ON SAND BEDS

GERHARD BARTZKE[AC], KARIN R. BRYAN[A], CONRAD A. PILDITCH[B] AND KATRIN HUHN[C]

[A]Department of Earth and Ocean Sciences, University of Waikato, Private Bag 3105, Hamilton 3240, New Zealand

[B]Department of Biological Sciences, University of Waikato, Private Bag 3105, Hamilton 3240, New Zealand

[C]MARUM – Center for Marine Environmental Sciences, University of Bremen, Leobener Straße, D-28359 Bremen, Germany

gbartzke@marum.de

Keywords: sediment mixtures; stabilization; annular flume; pore-space plugging; inflow blocking

ABSTRACT

In marine environments, sediments from different sources are stirred and dispersed, generating beds that are composed of mixed and layered sediments of differing grain sizes. Traditional engineering formulations used to predict erosion thresholds are however generally for unimodal sediment distributions, and so may be inadequate for commonly occurring coastal sediments. We tested the transport behavior of deposited and mixed sediment beds consisting of a simplified two-grain fraction (silt (D_{50} = 55 μm) and sand (D_{50} = 300 μm)) in a laboratory-based annular flume with the objective of investigating the parameters controlling the stability of a sediment bed. To mimic recent deposition of particles following large storm events and the longer-term result of the incorporation of fines in coarse sediment, we designed two suites of experiments: (1) "the layering experiment": in which a sandy bed was covered by a thin layer of silt of varying thickness (0.2 – 3 mm; 0.5 – 3.7 wt %, dry weight in a layer 10 cm deep); and (2) "the mixing experiment" where the bed was composed of sand homogeneously mixed with small amounts of silt (0.07 – 0.7 wt %, dry weight). To initiate erosion and to detect a possible stabilizing effect in both settings, we increased the flow speeds in increments up to 0.30 m/s. Results showed that the sediment bed (or the underlying sand bed in the case of the layering experiment) stabilized with increasing silt composition. The increasing sediment stability was defined by a shift of the initial threshold conditions towards higher flow speeds, combined with, in the case of the mixed bed, decreasing erosion rates. Our results show that even extremely low concentrations of silt play a stabilizing role (1.4% silt (wt %) on a layered sediment bed of 10 cm thickness). In the case of a mixed sediment bed, 0.18% silt (wt %, in a sample of 10 cm depth) stabilized the bed. Both cases show that the depositional history of the sediment fractions can change the erosion characteristics of the seabed. These observations are summarized in a conceptual model that suggests that, in addition to the effect on surface roughness, silt stabilizes the sand bed by pore-space plugging and reducing the inflow in the bed, and hence increases the bed stability. Measurements of hydraulic conductivity on similar bed assemblages qualitatively supported this conclusion by showing that silt could decrease the permeability by up to 22% in the case of a layered bed and by up to 70% in the case of a mixed bed.

INTRODUCTION

Estuaries are well known as highly dynamic coastal environments surrounded by densely populated areas and act as a filtering link on the sediment input brought by rivers and the sea. During fluvial sediment transport towards the sea, coarse-grained sediment fractions are usually trapped in the floodplains of rivers, while the fine fractions accumulate in the estuaries (Dyer 1994). Tidal currents and superimposed waves also supply sediment from the sea. During storm events, floodwaters carry new sediment as plumes into the estuary and previously deposited estuarine sediments are mixed and dispersed throughout the estuary. Differential settling rates create mixed and layered sediment beds of fine and coarse materials (Torfs 1997; Williamson 1991). Time-varying currents such as those caused by tides can also result in layered sediments, as fine materials are deposited over coarser compositions (Mitchener and Torfs 1997) during slack tide. Moreover, the sediments mobilized by dredging activities can often cause thin veneers of non-native sediment both as part of the dredging activity and also as part of the process of dredge-spoil dumping. Predicting the entrainment thresholds and erosion rates for these mixed sediment beds lies at the heart of understanding estuarine sediment dynamics, and such predictions are widely used across a number of fields ranging from our ability to reconstruct past sedimentary environments to understanding the impact of sediments on benthic communities following large storm events (Essink 1999; Leys and Mulligan 2011; Thrush et al. 2004; Zajac et al. 1998). In more applied cases, coastal engineers and managers rely on these predictions to manage port developments (drilling and dredging activities) and maintain navigation routes.

The threshold beyond which particles move is reached when the instantaneous fluid force (F_F) is larger than the resistance force (F_R) of the grain, which is a function of the particle weight (F_G), the particle angle of repose (φ), the lift force (F_L), and the drag force (F_D) (Allen 1970; Komar 1987; van Rijn 2007). This “initiation of motion” is classically defined by the empirically derived Shields curve (Shields 1936) as when the bed-shear stress exceeds the critical threshold for that particle size. The Shields curve was derived for uniform, homogeneous, noncohesive sediments of the same grain size (Soulsby 1997); it is less accurate for finer-grained beds (Hir et al. 2008; Mehta and Lee 1994). Thus Hjulström (1935; 1939) used observations in an attempt to develop a universal predictor of the critical erosion of sediments of a wide range of sizes (the “Hjulström Diagram”). This predictor indicated that fine sediments, in particular mud, are much harder to erode than sand. The common occurrence of muddy sediments in estuaries, which are typically composed of 60% silts (2 – 63 μm diameter) and 40% cohesive clays (< 2 μm diameter) (Manning et al. 2010; Winterwerp and Van Kesteren 2004) has focused research on developing critical threshold formulations for very fine-grained, cohesive, clay-rich

sediment compositions after removal of the sand fraction (Torfs 1997). The cause of these changes in entrainment characteristics towards higher bed stability in finer fractions is the influence of cohesion and biostabilization (Whitehouse et al. 2000). As shown by many studies on muddy, clay-rich sediments, cohesion (caused by electrostatic forces) binds together the clay minerals and increases the erosion resistance significantly (Alvarez-Hernandez 1990; Dyer 1989; Hir et al. 2008; Hir et al. 2011; Jacobs et al. 2011; Kamphuis 1990; Murray 1977; Panagiotopoulos et al. 1997; van Ledden et al. 2004). Biostabilization (Paterson 1994; Paterson et al. 1990; Paterson and Hagerthey 2001; Young and Southard 1978) is the influence of the activity of the micro-organisms (bacteria, microalgae, fungi) and macro-organisms (worms, molluscs, crustaceans), which can influence the sediment stability by binding sediment particles together, increasing erosion resistance, or break down sedimentary structure via bioturbation, decreasing erosion resistance (Karl and Novitsky 1988). An overview of the erosion formulations for estuarine mud can be found in Whitehouse et al. (2000) and Winterwerp and Van Kesteren (2004).

Many experiments on sand and mud beds have investigated these components separately to improve the understanding of the erosion behaviour (van Ledden et al. 2004) both in laboratory flumes flume (Black and Paterson 1997) and *in situ* (Amos et al. 1992; Whitehouse et al. 2000), yet natural estuarine sediments, which consist of both noncohesive (sand and coarser silt) and cohesive (finer silts and clay) fractions in various combinations, may behave quite differently than their component fractions. The different entrainment properties of the component particles cause different sediment fluxes relative to what would occur over uniform sediment beds of the component fractions (van Ledden 2002). Therefore mixtures may behave in ways not covered by the traditional relationships derived by Shields (1936) and Hjulström (1935; 1939). Recent studies on the threshold conditions of such mixed sediments so far have focused on the erosion behavior of sand and mud mixtures where the mud was composed of cohesive clay-rich compositions (van Ledden et al. 2004; Whitehouse et al. 2000). Laboratory experiments have shown a transition from noncohesive to muddy cohesive sediment with higher clay concentrations in the sediment beds (Alvarez and Hernandez 1990; Kamphuis 1990; Murray 1977). For example, Panagiotopoulos et al. (1997) identified, by progressively adding clay to sand, a critical clay content of 5 – 10% (by weight) increased the erosion threshold significantly. Others have observed a similar transition at a clay content of 5 - 15% (by weight) (van Ledden et al. 2004), while Torfs (1997) showed that adding 20 - 30% clay (by weight) to pure sand caused an order-of-magnitude increase of the critical bed shear stress. In general, the maximum value for increasing the critical bed shear stress depends on the grain size, porosity, and density of the sand (reviewed by Whitehouse et al. (2000)).

It is not only the cohesive properties of the finer fraction in mixed grain beds that causes the change in erosion behavior of the bed, but also the construction and packing of the bed and the existence of "network structures" (Whitehouse et al. 2000). At the surface of the sediment, fine grains can rest in the interstitial spaces of the rougher coarse grains, and thus be protected from erosion by the coarser grains (Komar 1987). This effect has been shown to be enhanced with increasing difference between the grain size of the two size fractions (NiÑo et al. 2003). However, most research has focused on the influence of the finer fraction on the erosion properties of coarser fraction. Mitchener and Torfs (1997) showed that sand stability increased when adding clay because the binding between the clay particles causes a denser matrix composition, which raises the erosion resistance. They demonstrated that the clay particles generated a cage-like network fully encompassing the sand grains. Consequently, the increased erosion resistance was a result of the binding influence and the developed clay cage. Panagiotopoulos et al. (1997) concluded that if the clay content exceeds 11 - 14%, the sand grains are no longer in contact with each other, which changes the particles angle of repose of mud, and therefore erosion resistance of the mixture is controlled by the clay characteristics. Van Ledden et al. (2004) reanalyzed the experiments of Panagiotopoulos et al. (1997) and Torfs (1997) and supported the idea that network structures influence the erosion resistance. Also, Hir et al. (2011) supported the concept that these network structures increase the erosion resistance. Furthermore, several theories have suggested that this texture phenomenon causes a reduction of the intergranular friction due to partial filling of the pore space (Hir et al. 2008; Panagiotopoulos et al. 1997; Torfs et al. 2000). However, the influences of sediment texture and the pore-space-filling network ("network structures") on the entrainment behavior of the sediments are not fully understood.

The literature on mixed sediments (sand and mud) suggests that clays are thought to be the only relevant factor in increasing the erosion resistance and hence the bed stability, due their cohesive properties and the ability to generate "network structures". For example, Jacobs et al. (2011) eroded artificially generated sand, mud, and silt mixtures and postulated that cohesiveness is more important to surface erosion and sediment strength than are packing density and drainage. However, silt is also a major part of the mud fraction in natural sediments. Silt is commonly found in many coastal environments of the world (e.g., along estuarine basins, estuarial river channels and mouths, artificial harbor basins (docks), navigational channels, and coastal shorelines and shelves (Dolphin and Green 2009; Healy 2002; van Rijn 2005; Winterwerp and Van Kesteren 2004). Further, Metha and Lee (1994) showed that cohesion is important only for silt particles less than 20 micrometers in size and cohesion is unlikely to play a role in silt-sand mixtures, suggesting that the role of other mechanisms such as the development of network structures might play a greater role in bed stability.

In contrast to previous studies, which have been limited to sand-dominated and clay-dominated mixtures, this paper explores effects of small amounts of noncohesive silt in a predominantly sandy bed on entrainment and transport and the potential role of silt in creating network structures and blocking the inflow of porewater. We use laboratory experiments in a small-scale annular flume to test the role of thin layers of silt blanketing the fine sand bed and the more common case of homogeneously mixed beds. These treatments were chosen to imitate respectively the recent deposition of particles following large storm events and the longer-term result of the incorporation of fines. Two suites of experiments were designed: (1) "the layering experiment": in which a layer of silt was deposited in increasing quantities on top of a homogeneous sand bed; and (2) "the mixing experiment": which used a mixed sediment bed consisting of sand and increasing amounts of silt. The stability of each bed was tested, using a unidirectional flow where the mean flow conditions were increased incrementally.

METHODS

2.1 Sediments

All sand used in the experiments (sampled from Pauanui Beach, New Zealand, 37°0'41.48" S 175°51'58.03" E) was dry sieved to 300 μm (D_{50}, average grain diameter) ranging from 210 to 310 μm; using an Endecott's sieve shaker, whereas the silt (sampled from Waikareao Estuary, Tauranga Harbour, New Zealand, 37°41'42.98" S 176°9'11.80" E) component was extracted from the bulk sample by wet sieving to D_{50} = 55 μm. Wet sieving had only a limited ability to constrain the size fraction, and the grain-size distribution of the silt fraction ranged from 0.8 to 200 μm (determined using a Laser Particle analyzer (Malvern Mastersizer 2000; Figure 1)). Note that the cohesive clay particles (< 2 μm) in the "silt" fraction constituted < 1.2% by volume and the cohesive silt particles (< 20 μm) were < 1.9% by volume.

2.2 Annular Flumes

The experiments were carried out using an annular laboratory flume (Figure 2). This was constructed with dimensions according to Widdows et al. (1998). The circular channel was 10 cm wide and was bounded by an outer (63 cm) and inner (43 cm) rim, resulting in a bed area of 0.17 m². At the maximum water level of 25 cm, 40 liters of artificial seawater (S = 30) were accommodated in the flume. A removable, rotating lid (45 cm diameter) driven by a 12 V motor was mounted on top of the flume, which caused a current motion of up to 0.30 m/s (55 rotations per minute; 1 is 0.00526 m/s (Jones et al. 2011)) The motor speed was controlled by a computer with Labview-based software which allowed the controlled variation of the flume flow speeds.

The concentration of suspended particulate matter (SPM) in the water column was recorded in millivolts by an optical back-scatter sensor (Seapoint turbidity meter; Seapoint Sensors Inc.) positioned 7.5 cm above the sediment bed (Figure 2) and was logged on a computer at 1 Hz. In mixed-grain suspensions, the OBS sensor preferentially senses the silt fraction (Green and Black 1999), and so the sensor was calibrated for each run individually. Water samples were extracted by suction through a sampling port (2 mm dia.) 7.5 cm above the sediment surface in order to calibrate the OBS sensor and to provide absolute measurements of the suspended load (following Widdows et al. 1998). The port was closed by a directional blocked center valve and connected by a plastic tube to a 50 ml Luer-Lok syringe (BD Plastipak). Samples for calibrating the OBS (for each run at each flow speed tested) were filtered through pre-weighed glass microfiber filters (GF/C 45 mm, Whatman) using a vacuum pump. The filters were prewashed in milli-q water to dissolve salts, then dried at 105 °C for 24 h and weighed.

2.3 Experimental Procedure

We designed two suites of experiments (summarized in Table 1): one in which a sand bed was covered by a thin layer of silt of varying thickness (1. the layering experiment), and one in which the bed was composed of sand mixed with small amounts of silt (2. the mixing experiment). Both experiments consisted of two phases. In Phase I the bed was allowed to settle and consolidate, and in Phase II, the velocity in the annular flume was increased to cause erosion. In each experiment the bed was prepared by creating a sediment bed 5 cm thick in the flume (sand in experiment 1, sand-silt mixture in experiment 2). After filling the channel with sediment, the bed was saturated with saltwater.To minimize any variations in surface elevation, which may promote the onset of erosion and add variability to the experiments, the bed was flattened by a scraper (sand bed in experiment 1, sand-silt mixture in experiment 2) before filling the flume. In the layering experiment the sand bed was scraped smooth prior to the sedimentation of the silt layer, and in the “mixed” treatments bed flattening occurred immediately after the sediment was placed in the flume. A sheet of bubble-wrap plastic, cut to the dimensions of the channel, was placed on top of the sediment to ensure that the bed was not disturbed by the inflow as the tank was filled. Subsequently, the motor, the OBS, and the rotating lid were installed.

During Phase I of each of the layering experiments, the six bed treatments were constructed by allowing 29, 118, 235, 353, 471, and 941 g/m² of silt to deposit in a thin layer on the bed ranging from 0.2, 0.6, 1.1, 1.8, 2.2, and 3 mm respectively. The ranges were chosen so that the lower levels (29; 118 g silt/m²) would fill the pore spaces but not cover the surface. The conversion to weight percentage (wt %) was calculated by considering a surface grab sample of 10 cm depth where the composition of the sample would correspond to 0.9, 1.4, 1.8, 3.7, and 7.3% (dry weight) silt. The silt was deposited on the sand bed by initially mixing it with 2 L of saltwater

and by shaking the container for a minute. To achieve the best possible dispersion in the flume, the silt mixture was poured gently into the flume with the motor running at 0.05 m/s for 5 min. The material was allowed to settle for 4 h by decreasing the flume flow velocity to 0.025 m/s. One run was undertaken with a 24 h settling time. It could be shown that after 4 h 99% of all silt which would have settled in 24 h was deposited, indicating that 4 h settling time was adequate. In the erosion Phase II the flume flow velocity was increased in steps of 0.025 m/s ranging from 0.025 to 0.30 m/s, with the exception of the change between 0.2 and 0.25 m/s, which was undertaken in one 0.05 m/s increment. Each flume-flow velocity increment was 15 min in length (Table 1). OBS calibration water samples were taken every 15 min. These flow speeds were chosen to characterize the environment on tidal sand flats (Leeder 1999; Wright et al. 1999) and were strong enough to initiate sediment transport in all treatments.

The mixing suite of experiments was made up of four runs, each with increasing quantities of silt added to the bed (120 g/m^3, 300 g/m^3, 600 g/m^3, 1200 g/m^3). Considering a surface grab sample of 10 cm depth of the sediment beds, these concentrations correspond to 0.74, 1.8, 3.7, and 7.4% (dry weight) silt. Similar to the layering experiments, the mixing experiments were divided into two phases. In Phase I, we added the mixed sand and silt to the flume and then allowed the bed to settle under no flow for 12 h. Phase II was the identical to that done in the layering experiments.

Photographs were taken at the beginning and end of the experiment, and video footage was collected during each experiment. This allowed qualitative observations of the erosion state of the bed, the formation of bedforms (the destabilization of the bed), the time that the surface silt layer was completely eroded, and the time at which the sand was first entrained from the bed. In these visual observations we defined “stable” as a bed in which the sand fraction was not mobilized at the highest flume flow velocity tested (0.30 m/s).

2.4 Near-Bed Hydrodynamics

We mapped the boundary-layer dynamics of three of the layering experiments (pure sand; 29 and 941 g/m^2) at flow speeds up to 0.20 m/s. To parameterize the bed shear stress (τ_0), we used a downward-looking SonTek MicroAcoustic Doppler Velocimeter (ADV). The ADV (Figure 2) was mounted onto a vertical racking system through the base plate into the middle of the channel (Jones et al. 2011). Because of this arrangement flow speeds higher than 0.2 m/s caused scour around the ADV and bed profiles were not measured. The spatial dimensions for a precise positioning near the bed was identified following Finelli et al. (1999). Each velocity profile was recorded at 25 Hz at 15 elevations from 0.5 cm up to 2.69 cm above the bed. The bed shear stress was calculated by using the turbulent kinetic energy (TKE) method (summarized in Kim et al. 2000 and Pope et

al. 2006). TKE describes the product of the absolute intensity of velocity fluctuations from the mean flume flow velocity and depends on the fluid density (ρ):

$$\text{TKE} = \frac{1}{2}\rho\left(\overline{u'^2} + \overline{v'^2} + \overline{w'^2}\right)$$

$$\tau_0 = C_1 \times \text{TKE}$$

$$C_1 = 0.19$$

where u' represents the fluctuating part of the flow in steam-wise direction and v' and w' the cross channel and vertical components of the flow. The ratio of bed shear stress (τ_0) to TKE is constant, and C_1 is the proportionality constant (Pope et al. 2006). The relationship between flow velocity and bed shear stress for the three treatments (pure sand, 29 and 914 g/m^2 silt) was linear (r^2 = 0.85-0.90; n = 7 - 9), and an analysis of covariance revealed no significant treatment effect (homogeneity of slopes p = 0.35; treatment p = 0.88) on boundary-layer flow characteristics. Consequently data from all three treatments were pooled to provide a single conversion formula for all treatments given by τ_0 (N/m^2) = 0.355×U (m/s) (r^2 = 0.88), where U is the depth-integrated flow speed in the flume.

In small annular flumes such as those used in these experiments, secondary flows are generated. The magnitude of the cross-stream flows in our flume are between 14 and 17% of the along-channel component (C. Pilditch, unpublished data). Note that this proportion does not vary with height above the bed or with along-channel flow speeds up to 0.45 m s^{-1}. Although the sediment transport dynamics are likely to be affected by these secondary flows, these were consistent across all treatments, and consequently comparisons between each experimental treatments are possible.

2.5 Hydraulic Conductivity

A constant-head permeameter was used (Klute and Dirksen 1986) to measure the hydraulic conductivity (k, m/s) of sediments in both the mixed and layered experiments. In cores (0.052 m diameter) a sediment column of 0.11 m was prepared in the same manner as the erosion experiment (allowing different amounts of silt to settle to the sand bed under gravity or being mixed into the bed) to mimic the range of bed compositions created in the flume. The value of k can be estimated from the height of the water column above the core (which remains constant), bed area and depth, and the time taken to collect a known volume of water passing through the bed. We constructed one example of each treatment and averaged several reading per core to estimate k.

2.6 Data Analysis

The stabilizing influence of silt on sand beds was analyzed by comparing the relationships between the suspended-particulate-matter concentrations (SPM), erosion rates, and critical bed shear stresses. OBS (mV) was converted to SMP (mg/l) using empirically derived relationships for each experiment. The coefficient of

determination (R^2) ranged from 0.91 to 0.96. The SPM time series following a step change in flow speed was well described by a hyperbolic tangent. Therefore, the sediment erosion rate (E), i.e., rate of change of suspended load in the water column, was modeled by the initial slope ab of the least-squares fit of the hyperbolic tangent model $y = a \tanh(bt)$ fitted to each 10 minute segment of SPM data (with constant velocity), where y is SPM concentration and t is time. The determination coefficients (R^2) of all experiments varied between 0.89 and 0.99, which was higher than the usually implemented linear regression analysis used by, for example, Widdows et al. (1998). With this model, the initial concentration reduces simply to $y = abt$, where the initial erosion rate (ab) and sediment concentration at large t asymptotes to $y = a$. The velocity needed to initiate transport of sand and/or silt at the sediment surface or destabilize the bed (as determined from video footage) was defined as the "critical velocity". The quantification of the critical bed shear stress (τ_c), was parameterized following Riethmüller et al. (1998) by using the relationship between the applied bed shear stress (τ_b) and sediment erosion rate. Fitting a linear regression line to these data at the first significant increase in erosion rate (> 35 mg/m²/s), allowed τ_c to be calculated as the intersection of regression line ($R^2 = 0.97 – 0.99$) with the x axis (bed shear stress).

RESULTS

Overall, the results show that silt increased the erosion resistance of the underlying sand (layering experiment 1) or mixed-grain bed (mixing experiment 2) and maintained the stability of the bed. In "low" silt concentration treatments (the layering experiments: 29 g/m², 118 g/m², 235 g/m², and the mixing experiment: 120 g/m³), no stabilization was observed, instead sand bedforms were generated at higher flow speeds (0.15 m/s, 0.20 m/s, 0.25 m/s) than in the pure-sand case. In contrast, in "high" silt concentration treatments (the layering experiments: 351 g/m², 471 g/m², 941 g/m², and the mixing experiment: 300 g/m³, 600 g/m³, 1200 g/m³) the underlying sand or mixed-sediment bed stabilized and no bedforms were observed. Furthermore, the measurements of hydraulic conductivity showed that with increasing silt content the hydraulic conductivity (k) decreased. Table 2 provides an overview of the sediment behavior derived from the flume experiments and the corresponding values of hydraulic conductivity. Additionally, photos showing one low and one high silt concentration run of both experiments are provided in Figure 3.

3.1 Hydraulic Conductivity

In both the layering and mixing experiments, the hydraulic conductivity decreased with increasing silt quantities, but the effect was greater in the mixed treatments (Table 2). For the layering experiments hydraulic conductivity decreased by 22%, from 0.00064 m/s for pure sand to 0.00045 m/s for the 9.5 g/m^2 treatment, but note that there was little detectable effect of silt on hydraulic conductivity in the range 0.3 - 2.0 g/m^2. In contrast,

silt mixed into the sediment produced a 70% reduction in hydraulic conductivity at 1200 g/m^3, and at 300 g/m^3 the reduction was comparable to that observed at the highest silt concentration used in the layering experiment.

3.2 The Layering Experiments

The change in suspended-sediment concentrations observed throughout the layering experiments as the flow speed increased (Phase II) are presented in Figure 4A. SPM concentrations decreased slightly below < 0.15 m/s because silt particles were still being deposited. At 0.15 m/s silt began to erode in all treatments (Figure 4A). After this critical threshold for initiation of silt erosion was exceeded, two classes of erosion behavior at silt concentrations < 235 g/m² (low) and > 352 g/m² (high) could be identified. Following each incremental change in flow speed, initial erosion was identified by a steep change in sediment concentration followed by an asymptotic decrease in the rate of change to constant concentration. The experiments with low levels of silt showed that the silt increased the threshold where the underlying sand began to move significantly (yellow, blue, and black lines in Figure 4A and Table 2). Visual observations indicated that the thicker the layer of deposited silt, the higher the threshold for sand movement. Therefore, the threshold for initial sand erosion was shifted to higher flow speeds (0.20 – 0.275 m/s) with increasing silt concentration (Figure 4A). Furthermore, visual observations indicated that this occurred when the layer of silt protecting the bed was eroded and the sand grains appeared to be exposed (thin silt layer in Figure 3, 1A). At higher flume flow velocities (> 0.275 m/s) the sand bed failed with the establishment of bed forms with 2 - 5 cm wavelength (Figure 3, 1B). In these cases, erosion of silt and sand was observed at the same time (Figure 4A). This sand and silt continued to be in put into suspension and accounts for the steep rise in suspended-sediment concentration (from 50 to 150 mg/l) in Figure 4A towards the end of the experiments.

The erosion rates of the low-silt layering runs have three stages (Figure 5A). Note that the erosion rates have been plotted against applied bed shear stress rather than flow speed, where 0.01 N/m² corresponds to a 0.05 m/s interval. In stage 1 there was no erosion until the initial silt erosion at 0.04 N/m². Then there was a gradual increase in erosion rate up to about 100 mg/m²/s (stage 2). The erosion rates increased up to a factor of 3, depending on initial silt concentration, and then declined, presumably as the surface layer of silt was depleted, and only sand grains were left to be suspended. In the last stage (3), when the bed shear stress reached 0.09 N/m², a strong increase of the erosion rates to 400 mg/m²/s for the low silt treatments occurred, which is related to continuous sand suspension in combination with the growth of bed forms (Table 2; Figure 3, 1B).

In contrast, the high silt concentrations (Figure 4A, brown, red, and green lines) stabilized the sand bed and no bed forms were observed (Table 2; Figure 3, 2B). The transition from a bed that becomes unstable at high flow speeds (low silt) and the ones that remain stable (high silt) corresponded to a silt concentration between 235

g/m² and 353 g/m². Similar to experiments with "low" concentrations, silt erosion was initiated at 0.15 m/s. As the flow speed increased, there was a continuous increase in SPM, and visually a decrease in the thickness of the silt layer on the bed surface was observed (compare Figure 3, 2A and 2B). Visual observations also revealed that silt was transported also as bed load on top of the sand bed. Even if all silt layering on the sediment appeared to be eroded (which occurred only at the highest flume flow velocity tested) and the sand surface was exposed, the remaining sand bed still stayed stable (compare Figure 3, 2A and 2B). In the final stages, the SPM concentration did not equilibrate as quickly after each change in velocity, and the erosion rate did not reach an asymptotic steady state within the 15-minute time frame. The transition to this decreasing pattern of erosion rate occurred at a lower flow speed (0.15 m/s) for the 471 g/m² and 941 g/m² experiments. At the highest flow speeds (> 0.275 m/s) and highest silt-layer thicknesses (the 471 g/m² and 941 g/m² runs), 0.5 - 1 cm wavelength silt bed forms appeared on top of the stable but partially exposed sand bed. The differences in SPM concentration between the 353 g/m², 471 g/m², and 941 g/m² experiments did not follow a consistent pattern. The SPM concentrations for the 471 g/m² experiments were always higher than the 941 g/m² experiments. The divergence in the erosion behavior of the 471 g/m² run occurs at the lower flow regimes (< 0.20 m/s), where only the silt is mobilized (Figure 4A).

The erosion rates for the "high" (353 g/m², 471 g/m², and 941 g/m²; brown, red, and green lines) silt layering runs differ from the pattern of the erosion rates for "low" silt concentrations in that the previously defined erosion stage (3) was not observed (Figure 5A). Following a steep increase which corresponds to the erosion of the silt layer at 0.04 – 0.05 N/m² (which occurred in all treatments, 100 – 1000 mg/m²/s), a trend towards a constant erosion rate or decreasing erosion rate seems to evolve at higher flow speeds. The flow speed where this flatting trend emerges is higher (> 0.07 N/m²) for larger silt amounts (compare yellow line and red line in Figure 5A). This flattening becomes particularly clear while considering the 118 g silt/m² curve (orange line). At this stage visual observation indicated that all silt was suspended, whereas the sand bed remained intact (Figure 3; 2B). The 353 g silt/m² (brown line) and 471 g silt/m² (red line) also follow the trend towards decreasing erosion rates because increasing the silt concentration extended the velocity range over which the silt layer was eroded. The last data point could not be collected due to a limited sensitivity range of the OBS sensor.

From visual observations it was determined that in the case of the pure sand bed the tested bed shear stresses resulted in primarily bed-load transport. In this case, the sand was not resuspended to the height of the sensor in sufficient quantities for detection (Figure 4). Therefore, the derived erosion rate change resulting from increased bed shear stresses were compared with the predicted erosion behavior of pure silt (black dashed line in Figure 5) and pure sand (black dashed and dotted line in Figure 5) based on the erosion rates estimated from

published relationships. The erosion functions of pure silt and sand were derived based on the formulations described by Hir et al. (2008) and Mehta and Parchure (2000):

$$E = M\left(\frac{\tau_b - \tau_c}{\tau_c}\right)^n,$$

where E corresponds to the erosion rate (mg/m²/s), M and n are erosion-rate constants which were optimized from calibration (M-sand = 20; M-silt = 500; n = 1.5; i.e. van Rijn 2007) whereas τ_c represents the critical bed shear stress (N/m²) respectively. The critical bed shear stress for silt is 0.03 N/m² and was derived from the erosion-rate plots following Riethmüller et al. (1998) and was found to be equal for the initial silt erosion for all experiments. In contrast, the critical bed shear stress of sand, 0.05 N/m², was derived by the Shields curve found in Soulsby (1997). Our experimental results indicate that the erosion characteristics of the layered bed lie between these two extremes, as expected.

3.3 The Mixing Experiments

The SPM recordings taken at different flow speeds collected throughout the mixing experiments are illustrated in Figure 4B. Both visual observations and the SPM measurements confirmed that silt erosion took place only when the flow speed exceeded 0.15 cm/s. Experiments with “low” silt concentrations in the bed (120 g/m³; black line in Figure 4B) differ from experiments with “high” silt concentrations (> 300 g/m³; blue, yellow, and brown lines in Figure 4B). The run with low bed silt concentration did not level off to a constant suspended-sediment concentration, instead it was characterised by a steep increase up to 180 mg/l, which occurred at relatively high flow speeds (0.20 – 0.30 m/s). Visual observation showed that sand erosion was initiated at 0.20 m/s and was immediately accompanied by the appearance of 2 – 3 cm wavelength bed forms which were fully established during the 0.30 m/s flow interval (compare Figure 3; 3A and 3B). During the “high” silt concentration runs (blue, yellow, and brown lines in Figure 4B), the sediment bed remained stable and no generation of sand bedforms could be observed (compare Figure 3; 4A and 4B). In contrast to the layering experiments, visual observations indicated that silt was suspended directly out of the sand bed. Moreover, SPM increased less with increasing flow speed. Therefore the erosion rate (Figure 5B) decreased when there were increased levels of silt mixed into the bed. In particular, the transition between higher erosion rates and lower erosion rates (Figure 5B) occurred at different flow speeds (0.15 – 0.175 m/s) in the 300 and 600 g/m³ experiments. In contrast, the 1200 g/m³ runs were characterised by a low erosion rate and minor changes in SPM.

The erosion rates calculated from the mixing experiments (Figure 5B) highlight the effect of a decreasing erosion potential during higher current velocities by increasing silt concentrations in the bed.

Experiments with “low” silt concentrations (Figure 5B, black line) are characterized by a continuous rise of the erosion rates. Silt began to be eroded at 0.04 N/m² and was followed by sand erosion beginning at 0.08 N/m². In comparison, in “high” bed-silt concentrations (Figure 5B, blue, yellow, and brown lines), the erosion rate of the 300 and 600 g/m³ experiments peaked between 0.04 N/m² and 0.06 N/m², followed by a decline towards zero. Visual observations indicated at this stage that no more additional silt was suspended. Suprisingly, even up to bed shear stresses of 0.1 N/m², the erosion rates for the highest bed-silt concentrations (1200 g/m³) show only a minor increase in SPM. Further, the erosion rates of the mixing experiments are compared with the predicted erosion behavior of pure silt (black dashed line in Figure 5B) and sand (black dashed and dotted line). The results show that the erosion characteristics of the mixed bed lie approximately between the predicted erosion rates for pure sand (dashed line, Figure 5) and pure silt (dash-dot line in Figure 5). At high bed shear stresses, the mixed sediment bed erodes at a lower rate than expected for a pure sand bed.

DISCUSSION

The annular-flume experiments show that silt either deposited on top of a sand bed or mixed into a sand bed has a stabilizing effect on the sand bed. The threshold conditions for initiation of motion of sand were shifted to higher flow speeds for beds containing silts compared to initial threshold conditions for a pure sand bed. Even a relatively small amount of silt that was either deposited out of suspension (1.4 silt wt %) or mixed into the sediment bed (0.18 silt wt %) induced sediment stabilization. Furthermore, the measurements of hydraulic conductivity showed a significant decrease in permeability in mixed sand-silt beds (Table 2). Therefore, our results show that even minor changes to the silt composition of the bed, and the distribution of the silt within the bed, can cause dramatic changes to the erosion rates and to the hydraulic conductivity, and hence, increase the bed stability. These changes to erosion rates encompass the entire range between predicted rates for pure sand and pure silt.

All studies so far which focused on mud and sand mixtures (Alvarez-Hernandez 1990; Dyer 1989; Kamphuis 1990; Mitchener and Torfs 1997; Murray 1977; Panagiotopoulos et al. 1997; Raudkivi 1990; Torfs et al. 2000; van Ledden et al. 2004) have noted an increased erosion resistance (compared to pure sand) when treating sand (noncohesive) with mud (in particular cohesive clays) in various compositions. The transition from sandy (noncohesive) to more stable muddy (cohesive) erosion behavior occurs at clay contents ranging between 3 and 15% (reviewed in Whitehouse et al. 2000). However, our results also show that silt layered on top of a sand bed (the layering experiments) stabilized the sediment with a minimum silt concentration of 353 g silt/m², which corresponds to only 1.4% silt (wt %) (considering comparable bed samples of 10 cm depth). This is comparable to previous mud experiments. Moreover, when silt was mixed into sand (mixing experiments), the

sediment was stabilized at a minimum concentration of 300 g/m³, i.e., 0.18% silt (wt %), which is much lower than previous findings (see above, albeit for mud). Our results clearly demonstrate that concentrations of lower noncohesive silt are required to increase the erosion resistance than in the case of cohesive mud.

Prior studies have shown that the main physical controls on the erosion of sediments are the mineralogy, grain-size distribution, density, and cohesion (Allen 1970; Hir et al. 2008; McCave 1984) as well as "network structures" (Whitehouse et al. 2000). Due to the fact that our samples were separated from the cohesive clay fraction by sieving, cohesion is unlikely to influence the stabilization behavior of our silt-sand treated sediment beds (Winterwerp and Van Kesteren 2004). Furthermore, Mehta and Lee (1994) showed that the cohesion of silt is significant only for particles smaller than 20 microns, whereas our samples have a median diameter of 55 μm. The cohesive silt particles < 20 μm (1.9 vol. %) and cohesive clays < 2 μm (1.2 vol. %) were only a minor part of the total volume fraction of our silt component and are unlikely to have caused a cohesive influence on the erosion behavior.

Following the hypothesis that a texture-induced sand-bed stabilization, where the clay particles fill the pore spaces between the sand grains, can create a "cage-like" structure (Hir et al. 2008; Hir et al. 2011; Mitchener and Torfs 1997; Panagiotopoulos et al. 1997; van Ledden et al. 2004; Whitehouse et al. 2000), we postulate that the noncohesive silt in our treatments is filling the sand matrix. We did not measure these structures directly, but the hydraulic conductivity measurements decreased with added silt, and thus, also possibly a decrease in permeability, in both experimental setups (Table 2). This indicates that the quantity of silt particles controls the blockage of the flow through the sediment bed and may explain the increase in sediment stability caused by added silt in the flume experiments. Furthermore, there was a larger decrease in hydraulic conductivity in the case of the mixed sediment cores as compared to the layered cores with increasing silt content. This also corresponds with the findings of the flume experiments, which showed that silt mixed into the sediment beds appeared to cause more stability than layered sediment beds. This effect may reduce the pore-water inflow as indicated by the measurements of hydraulic conductivity, but also minimizes changes in the pore water pressure, and hence, reduces the effective stress in the bed (Eisbacher 1996).

Panagiotopoulos et al. (1997) suggested that the erosion resistance is increased by infilled pockets increasing the internal particle angles of repose between fines and sand. In a sediment bed composed of coarse sand particles, all sand particles are more or less in contact with each other. When fine clay particles are mixed into the matrix of the coarse sand bed, the distances between the coarser grains is increased due to the filling of the pore space with finer particles, slightly increasing the pivoting characteristics, i.e., particle angle of repose. So when finer particles were included in the pore spaces, the bed was more resistant to erosion. In addition, we

suggest that the filling would also decrease the surface roughness of the bed by filling in the hollows between grains. NiÑo et al. (2003) show that fine-grained particles are less easily entrained when they are hidden in the pore spaces between coarser particles, and thus the roughness of the coarse bed can reduce the erosion rate of fine particles in a mixed-grain bed. Although we measured erosion rates and did not directly measure entrainment thresholds, our results suggest that the change in erosion thresholds caused by mixed-grain-size beds (shown in NiÑo et al. 2003) is entirely dependent on the quantity of fine sediment relative to coarse, and the erosion rates can range from erosion rates of a pure silt bed to much lower values.

A conceptual model that highlights our understanding of the stabilizing influence of silt on sand bed is presented in Figure 6. This is based on former studies which suggested that fine particles fill the voids between large grains to generate a more densely packed matrix affecting the erosion threshold. Our experiments can be analyzed in more detail within the framework of this conceptual model.

4.1 Initial Response

The initial response of the bed to increasing flow speeds was the removal of the surface silt layer in the case of the layering experiments and removal of the easily available surface silt in the case of the mixing experiments. In the case of the layering experiments, this corresponds to entrainment of grains for a bed of the same grain size, and so the roughness elements of the sand should have no effect on the entrainment process (NiÑo et al. 2003). It is possible to determine when the surface layer is removed, when the erosion-rate curves deviate from the pure-silt case (dashed black line in Figures 5A and B). Before this point, the silt eroded following the theoretical curve for noncohesive silt. This provides some confirmation of our assumption that the silt is not cohesive. In the case of layers of silt of 235 g/m^2 or less, this silt layer was removed immediately.

Initial erosion of the silt in the mixing experiments varied depending on treatment. The silt was most easily eroded in the 300 g/m^3 case but not in the cases with higher silt fractions. Erosion from the mixed bed would depend on the surface roughness and the flow through the pore spaces (Figure 3; 4A; 6C). Roughness influences entrainment by changing the particle angle of repose, changing the bed shear stress and the degree to which the fine particles can be hidden by the coarser particles (NiÑo et al. 2003). The 300 g/m^3 may cause the roughest bed, yet large enough separation between sand grains that hiding is less important (Figure 6C). When the bed silt concentration increases even more, the separation between grains becomes greater, which may reduce the roughness and decrease the particle angle of repose of the sand grains, and cause the erosion rate to drop (Panagiotopoulos et al. 1997; Wiberg and Smith 1987). The influence of pore-space blocking, which inhibits flow through the bed, may also influence these higher bed-silt concentration more. This is supported by

the dramatic drop in hydraulic conductivity at these silt concentrations (Table 2). However, we do not have direct evidence of the effect of silt on bed roughness, so this interpretation remains conjecture at this point.

4.2 Blocked Pore Spaces

When the easily available silt was eroded from the bed (either from the surface layer or from between the surface grains), the erosion characteristics depended on how the silt was incorporated into the bed. In this case, the bed was stable when silt was contained within the pore spaces of the sand (Figure 3; 2B and 4B), and the flow that normally occurs between the sand grains (and helps the entrainment processes) was blocked. This occurred during both experiments, either when the surface layer of silt had been removed or when there was sufficient silt incorporated in the bed. With respect to our conceptual model (Figure 6), we assume that bed stabilization (Figure 3; 2B and 4B) occurs when a "blocked layer" in Figures 6B and D evolved, whereby the smaller, denser silt particles filled the pore spaces between sand grains either by deposition or mixing until a stage of saturation was achieved, i.e., pore-space plugging caused a blockage of the inflow (flow vectors in Figure 6B and D). This occurred during both experiments, either when the surface layer of silt had been removed (Figure 3; 2B) or when there was sufficient silt incorporated in the bed (Figure 3; 4B), which was also indicated by the decrease in hydraulic conductivity. Consequently, this would take place in the experiments with significant silt coverage of 353 g/m² (brown line in Figure 5A) and 300 g/m³ silt content (blue line in Figure 5B) for the mixed case. Furthermore, this filling of the surface pore space and coating of sand particles (Mitchener and Torfs 1997; Panagiotopoulos et al. 1997) maintains smoother surface conditions (Figure 3; 2B and 4B), which, in turn, would also cause a blockage of the inflow (flow vectors in Figure 6B and D) and hence, reduce erosion rates. Moreover, this is accompanied by the reduction of the drag and lift forces acting on the sand particles as suggested by Komar (1987) and Panagiotopoulos et al. (1997).

In terms of the layering experiments, possible evidence for the existence of the blocked inflow is that when the surface layer of silt is removed (compare Figure 3; 2A and 2B), the erosion rate does not immediately return to the erosion rate of pure sand, but instead depends on the initial depth of the layer of silt (note the difference in erosion rate between the brown line 353 g/m² and yellow line 235 g/m² in Figure 5A). This increase in the effectiveness of the blocked layer may be due to the internal compaction within the pockets, which may have more of an effect when the initial silt layer is thicker. It could also be that the underlying sand bed is exposed at higher flow speeds when the initial silt layer is thicker, and so the higher flow speeds might cause structural strengthening of the blocked layer. Therefore, a possible explanation could be that the "blocked layer" either becomes thicker or increases in depth and so is more pronounced, causing a higher stability due to denser network structures (Torfs 1997).

501 The SPM concentration differences between the 471 g/m² and 941 g/m² runs (Figure 4A) of the layering
502 experiments could be explained by the evolution of a blocked layer. We assume that at higher flow speeds the
503 hydrodynamic pressure on the layer forced the silt particles to migrate in the pore space of the underlying sand
504 bed. In the case of an initial thicker silt layer, i.e., the 941 g/m² run, (Figure 3; 2A), additional sediment loading
505 might enhance this effect, and hence, could cause structural strengthening. A possible explanation could
506 therefore be that the "blocked layer" becomes thicker, causing higher stability due to denser network structures
507 (Torfs 1997), similar to self-weight consolidation processes, which have been observed to decrease erosion
508 potential (Whitehouse et al. 2000). It is interesting to note that a surface silt layer caused only a small decrease in
509 hydraulic conductivity (Table 2) compared to the case of a mixed bed. This might be because without the
510 dynamic pressure caused by the overlying flow, silt is not forced into the underlying sand bed. In the case of the
511 mixed experiments, the blocked layer is not limited to the surface (Figure 6D), which may explain why erosion
512 rates were generally lower relative to the layered experiments.

513 *4.3 Bed Destabilization - "Undersaturated" Pore Space*

514 In cases when a very thin layer of silt is deposited on top of a sand bed (Figure 3; 1A), and also when
515 only a small amount of silt is incorporated into the bed (Figure 3; 2A), the bed destabilizes and is eroded at the
516 higher flow speeds (compare with bed forms in Figure 3; 1B, 2B). This could be caused by an "undersaturated"
517 pore space (Figure 6A) where silt was deposited or mixed (Figure 6C) in concentrations too small to be able to
518 fill the pore space of the sand bed. Consequently, silt was immediately eroded and was not able to protect the
519 exposed sand grains from inflow (deep flow vectors in Figure 6A and 6C). Moreover, the sand grains were more
520 exposed to the flow (i.e., surface appears rougher in Figure 3; 1A and 3A), which would cause rougher surface
521 texture, which in turn would enhance inflow into the sediment bed and increase the likelihood of sand erosion
522 (Figure 6A and 6C). This was also supported by relatively high values of hydraulic conductivity. It is interesting
523 to note that when silt was removed (yellow, blue, and black lines in Figure 5A; and black line in Figure 5B), the
524 sand bed eroded approximately like a pure sand bed, indicating that the pore-space blockage was either non-
525 existent or very shallow and easily flushed out under increasing flow speeds. Our flume experiments ceased at
526 0.30 m/s, so it is possible that the thicker layer treatments and the sediment beds mixed with greater fractions of
527 silt might eventually also become unblocked and begin to erode.
528
529 Secondary currents are nearly always present in small annular flumes due to the geometry and methods
530 used to generate the flow. Although our results are affected by these flow patterns and may not be comparable to
531 results from the field and other flumes, these flow patterns are not dependent on treatment, and so our results

should be comparable between treatments. Pope et al. (2006) used a similar setup and compared *in situ* field data collected on intertidal flats with their annular-flume results. They showed that the findings derived with their annular flume were environmentally realistic and representative of the dynamic sediment conditions observed in the field. There are limitations to this study, e.g., the difficulty in resolving flows in a compressed laboratory boundary layer, the inability to differentiate between suspended sand and silt by the OBS, and the difficulty in resolving the behavior of the "blocked layer", and the evolution of surface roughness during the bed stabilization process on a grain-scale level. A combined ABS-OBS (where ABS is an acoustic backscatter sensor) in the flume channel may give considerable added insight into the processes of erosion and suspension in experiments of this kind (Green and Black 1999). Despite these shortcomings, our study shows clear evidence of the effect of noncohesive fine particles on sand-bed stabilization, and provides possible explanations for our observations which can guide future studies.

CONCLUSIONS and OUTLOOK

We designed two suites of experiments to investigate the influence of silt stabilization on a sand bed: (1) the layering experiment, where a sandy bed was covered by a thin layer of silt of varying thickness, and (2) the mixing experiment, where the bed was composed of sand mixed with small amounts of silt. All samples were tested in an annular flume for their stability effects using incrementally increasing flow speeds up to 0.30 m/s. Our results show that a silt layer that was deposited on top of a sand bed stabilized the bed when the concentration was less than 353 g/m^2, which corresponds to 1.4% silt (wt %). In contrast, a silt mixed sediment bed was stabilized within a minimum concentration of 300 g/m^3, i.e., 0.18% silt (wt %). Therefore, the stabilization behavior is sensitive to how the silt is distributed within the bed. Furthermore, we could show that much lower silt concentrations are required to stabilize a sand bed in comparison to studies on muddy cohesive sediments. We suggest that the bed stabilization is controlled by the amount of silt which was filling the pore space i.e., "pore-space blocking" of the sand bed and the influence of silt on bed roughness. The effect of pore-space blocking could possibly be caused the development of a horizon of the "blocked layer" which blocked the inflow into the sediment bed, maintained smooth surface conditions, and hence caused sediment stabilization. However, more research on the stabilizing process of silt and sand compositions and establishment of the "blocked layer" needs to be undertaken, especially on micro scale level, which could be accomplished by high-resolution, 3D numerical "flume tank" models adopting the general settings of the empirical experiments. For example, two independent numerical simulation techniques can be coupled, using the finite-difference method (FDM) and the distinct-element method (DEM) to simulate sediment transport processes on a grain-by-grain

562 basis in aquatic environments. (e.g. Cundall and Hart 1989; Cundall and Strack 1979, 1983; Itasca 2004; and
563 Kock and Huhn 2007).

564 Given that the bed stabilization is highly sensitive to small silt concentrations, manipulating the layering
565 structure may be a useful tool for the dredging and sea-bed structure industry in order to stabilize dumped
566 sediment at the seafloor. Often when obtaining bed samples in the field (e.g., from grab samples or even short
567 cores), the surface structure is destroyed and even homogenized during sampling. If we were to take a surface
568 grab sample of 10 cm depth of a sediment bed and measure the composition of the disturbed sample (in which
569 the original structure was destroyed) this minimum condition for stabilization in each case would correspond to
570 1.4% silt (wt %) for a layered sediment bed and 0.18% silt (wt %) for a mixed composition. An understanding of
571 the layering structure and its role in controlling sediment stabilization not only has engineering applications, but
572 many benthic fauna rely on the ability to access water-column nutrients and remove excreted material through
573 movement of water through pore spaces, and the pivotal role of silt in blocking this process highlights the danger
574 of natural and anthropogenically driven shifts to the particle size distribution of inputs of terrestrial sediment to
575 estuaries.

576 # ACKNOWLEDGMENTS

577 This work has been funded through Deutsche Forschungs Gemeinschaft-International Research
578 Training Group “INTERCOAST “. We thank Dr. Christian Winter, Dr. Willem de Lange, Annette Rodgers,
579 Rafael Guedes, Hannah Jones, Hazel Needham, Lina Podszun, Jannis Kuhlmann, Linda Wenk, Lutz Torbahn,
580 Christopher Daily, Dr. Giovanni Coco, Prof. Dr. Burghard Flemming, and the INTERCOAST research student
581 Antonia Ruppel, who freely shared their expertise. We also acknowledge the constructive comments of two
582 anonymous reviewers, which greatly improved the manuscript. The Hanse Wissenschaftskolleg supported a
583 research stay of Dr. Karin R. Bryan at Bremen University.

584

REFERENCES

Allen, J.R.L., 1970, Physical Processes of Sedimentation: London, Unwin University Books, 248 p.

Alvarez-Hernandez, E.M., 1990, The Influence of Cohesion on Sediment Movement in Channels of Circular Cross-Section: University of New Castle upon Tyne, UK, p. 367.

Amos, C.L., Grant, J., Daborn, G.R., and Black, K., 1992, Sea Carousel - A Benthic, Annular Flume: Estuarine, Coastal and Shelf Science, v. 34, p. 557-577.

Black, K., and Paterson, D.M., 1997, Measurement of the Erosion Potential of Cohesive Marine Sediment: A Review of Current in Situ Technology: Journal of Marine and Environmental Engineering, v. 4, p. 43-83.

Dolphin, T.J., and Green, M., 2009 Patterns of Wave-Orbital Speed and Skin Friction Under Estuarine (Fetch-Limited) Waves: Journal of Coastal Research, v. 56, p. 178-182.

Dyer, K.R., 1989, Sediment Processes in Estuaries: Future Research Requirements: Journal of Geophysical Research, v. 94, p. 14, 327-14, 339.

Dyer, K.R., 1994, Estuarine Sediment Transport and Deposition *in* Pye, K., ed., Sediment Transport and Depositional Processes: Oxford, U.K., Blackwell Scientific Publications, p. 193-218.

Eisbacher, G.H., 1996, Einführung in die Tektonik: Stuttgart, Spektrum Akademischer Verlag; Thieme; Enke, 374 p.

Essink, K., 1999, Ecological Effects of Dumping of Dredged Sediments; Options for Management: Journal of Coastal Conservation, v. 5, p. 69-80.

Finelli, C.M., Hart, D.D., and Fonseca, D.M., 1999, Evaluating the Spatial Resolution of an Acoustic Doppler Velocimeter and the Consequences for Measuring Near-Bed Flows: Limnology and Oceanography, v. 44, p. 1793–1801.

Green, M.O., and Black, K.P., 1999, Suspended-Sediment Reference Concentration Under Waves: Field Observations and Critical Analysis of two Predictive Models: Coastal Engineering, v. 38, p. 115-141.

Healy, T., 2002, Chapter Fourteen: Muddy Coasts of Mid-Latitude Oceanic Islands on an Active Plate Margin - New Zealand, *in* Healy, T., Wang, Y.A., Healy, eds., Proceedings in Marine Science, Volume 4: Amsterdam, Elsevier, p. 347-374.

Hir, P.L., Cann, P., Waeles, B., Jestin, H., and Bassoullet, P., 2008, Chapter 11: Erodibility of Natural Sediments: Experiments on Sand/Mud Mixtures from Laboratory and Field Erosion Tests, *in* Kusuda, T., Hiroyuki, Y., Spearman, J., Gailani J.Z., eds., Proceedings in Marine Science, Volume 9: Amsterdam, Elsevier, p. 137-153.

Hir, P.L., Cayoccaa, F., and Waeles, B., 2011, Dynamics of Sand and Mud Mixtures: A Multiprocess-Based Modelling Strategy: Continental Shelf Research, v. 31, p. 135-149.

Hjulström, F., 1935, Studies in the Morphological Activity of Rivers as Illustrated by the River Fyris:Geological Institute of Uppsala, Bulletin v. 25, p. 221–527.

Hjulström, F., 1939, Transport of Detritus by Moving Water Recent Marine Sediments, *in* Trask, P.D., ed., Recent Marine Sediments; A Symposium: Tulsa Oklakoma, American Association of Petroleum Geologists: New York, London, T.Murby & Co., Reprinted 1968 by Dover Publications, p. 3-31.

Jacobs, W., Hir, P., Van Kesteren, W., and Cann, P., 2011, Erosion Threshold of Sand-Mud Mixtures: Continental Shelf Research, v. 31, p. S14-S25.

Jones, H.F.E., Pilditch, C.A., Bryan, K.R., and Hamilton, D.P., 2011, Effects of Infaunal Bivalve Density and Flow Speed on Clearance Rates and Near-Bed Hydrodynamics: Journal of Experimental Marine Biology and Ecology, v. 401, p. 20-28.

Kamphuis, J.W., 1990, Influence of Sand or Gravel on the Erosion of Cohesive Sediment: Journal of Hydraulic Research, v. 28, p. 43-53.

Karl, D.M., and Novitsky, J.A., 1988, Dynamics of Microbial Growth in Surface Layers of a Coastal Marine Sediment Ecosystem: Marine Ecology Progress Series, v. 50, p. 169-176.

Kim, S.C., Friedrichs, C.T., Maa, J.P.Y., and Wright, L.D., 2000, Estimating Bottomstress in Tidal Boundary Layer from Acoustic Doppler Velocimeter Data: Journal of Hydraulic Engineering, v. 126, p. 399–406.

Klute, A., and Dirksen, C., 1986, Hydraulic Conductivity and Diffusivity: Laboratory Methods, *in* Klute, A., eds., Methods of Soil Analysis, Part 1 - Physical and Mineralogical Methods: American Society of Agronomy-Soil Science Society of America, Agronomy Monograph, Volume 9, p. 687-734.

Komar, P.D., 1987, Selective Grain Entrainment by a Current from a Bed of Mixed Sizes: A Reanalysis: Journal of Sedimentary Research, v. 57, p. 203-211.

Leeder, M.R., 1999, Sedimentology and Sedimentary Basins: From Turbulence to Tectonics: Oxford, U.K., Blackwell Science, 608 p.

Leys, V., and Mulligan, R.P., 2011, Modelling Coastal Sediment Transport for Harbour Planning: Selected Case Studies, *in* Ginsberg, S.S., 2 ed., Sediment Transport, http://www.intechopen.com/articles/show/title/modelling-coastal-sediment-transport-for-harbour-planning-selected-case-studies.

Manning, A.J., Baugh, J.V., Spearman, J.R., and Whitehouse, R.J.S., 2010, Flocculation Settling Characteristics of Mud: Sand Mixtures: Ocean Dynamics, v. 60, p. 237-253.

McCave, I.N., 1984, Erosion, Transport and Deposition of Fine-Grained Marine Sediments, Geological Society of London, Special Publications, v. 15, p. 35-69.

Mehta, A.J., and Lee, S.-C., 1994, Problems in Linking the Threshold Condition for the Transport of Cohesionless and Cohesive Sediment Grain: Journal of Coastal Research, v. 10, p. 170-177.

Mehta, A.J., and Parchure, T.M., 2000, Surface Erosion of Fine-Grained Sediment Revisited, *in* Flemming, B.W., Delafontaine, M.T., and Liebezeit, G., eds., Proceedings in Marine Science, Volume 2: Amsterdam, Elsevier, p. 55-74.

Mitchener, H., and Torfs, H., 1997, Erosion of Mud/Sand Mixtures: Coastal Engineering, v. 29, p. 1-25.

Murray, W.A., 1977, Erosion of Coarse Sand-Clayey Silt Mixtures: American Society of Civil Engineers, Proceedings, Journal of the Hydraulics Division, v. 103, no. HY10, p. 1222-1227.

NiÑo, Y., Lopez, F., Garcia, M., 2003, Threshold for Particle Entrainment into Suspension: Sedimentology, v. 50, p 247-263.

653 Panagiotopoulos, I., Voulgaris, G., and Collins, M.B., 1997, The Influence of Clay on the Threshold of Movement of Fine
654 Sandy Beds: Coastal Engineering, v. 32, p. 19-43.
655 Paterson, D.M., 1994, Biological Mediation of Sediment Erodibility: Ecology and Physical Dynamics, *in* Burt, N., Parker, R.,
656 Watts, J., eds., Cohesive Sediments, v. 1, Chichester, John Wiley, p. 215-229.
657 Paterson, D.M., and Hagerthey, S.E., 2001, Microphytobenthos in Contrasting Coastal Ecosystems: Biology and Dynamics:
658 *in* Reise, K., eds., Ecological Comparisons of Sedimentary Shores. Ecological Studies, v. 151, Berlin, Springer, p.
659 105-125.
660 Paterson, D.M., Crawford, R.M., and Little, C., 1990, Subaerial Exposure and Changes in the Stability of Intertidal Estuarine
661 Sediments: Estuarine, Coastal and Shelf Science, v. 30, p. 541-556.
662 Pope, N.D., Widdows, J., and Brinsley, M.D., 2006, Estimation of Bed Shear Stress Using the Turbulent Kinetic Energy
663 Approach - A Comparison of Annular Flume and Field Data: Continental Shelf Research, v. 26, p. 959-970.
664 Raudkivi A.J., 1990, Loose Boundary Hydraulics: Oxford, U.K., Pergamon, p. 497.
665 Riethmüller, R., Hakvoort, J.H.M., Heineke, M., Heymann, K., Kühl, H., and Witte, G., 1998, Relating Erosion Shear Stress
666 to Tidal Flat Surface Colour: Geological Society of London, Special Publications, v. 139, p. 283-293.
667 van Rijn, L.C., 2005, Estuarine and Coastal Sedimentation Problems: International Journal of Sediment Research, v. 20, p.
668 39-51.
669 van Rijn, L.C., 2007, Unified View of Sediment Transport by Currents and Waves. I: Initiation of Motion, Bed Roughness,
670 and Bed-Load Transport: Journal of Hydraulic Engineering, v. 133, p. 649-667.
671 Shields, A., 1936, Anwendung der Ähnlichkeitsmechanik und der Turbulenzforschung auf die Geschiebebewegung:
672 Mitteilungen Preußische Versuchsanstalt für Wasserbau und Schiffbau, v. NW 87.
673 Soulsby, R., 1997, Dynamics of Marine Sands. A Manual for Practical Applications: London, Thomas Telford Publishing, p.
674 249.
675 Thrush, S.F., Hewitt, J.E., Cummings, V.J., Ellis, J.I., Hatton, C., Lohrer, A., and Norkko, A., 2004, Muddy Waters:
676 Elevating Sediment Input to Coastal and Estuarine Habitats: Frontiers in Ecology and the Environment, v. 2, p.
677 299-306.
678 Torfs, H., 1997, Erosion of Mixed Cohesive/Non Cohesive Sediments in Uniform Flow, *in* Burt, N., Parker, R., and Watts, J.,
679 eds., Cohesive Sediments, v. 1, Chichester, John Wiley, p. 245–252.
680 Torfs, H., Jiang, J., and Mehta, A.J., 2000, Assessment of the Erodibility of Fine/Coarse Sediment Mixtures, *in* McAnally,
681 W.H., and Mehta, A.J., eds., Proceedings in Marine Science, Volume 3: Amsterdam, Elsevier, p. 109-123.
682 van Ledden, M., 2002, A Process-Based Sand-Mud Model, *in* Winterwerp, J.C., and Kranenburg, C., eds., Proceedings in
683 Marine Science, Volume 5: Amsterdam, Elsevier, p. 577-594.
684 van Ledden, M., van Kesteren, W.G.M., and Winterwerp, J.C., 2004, A Conceptual Framework for the Erosion Behaviour of
685 Sand-Mud Mixtures: Continental Shelf Research, v. 24, p. 1-11.
686 Whitehouse, R., Soulsby, R., Roberts, W., and Mitchener, H., 2000, Dynamics of Estuarine Muds; A Manual for Practical
687 Applications: London, Thomas Telford Publishing, 210 p.

688 Wiberg, P.L., and Smith, J.D., 1987, Calculations of the Critical Shear Stress for Motion of Uniform and Heterogeneous
689 Sediments: Water Resources Research, v. 23, p. 1471-1480.
690 Widdows, J., Brinsley, M.D., Bowley, N., and Barrett, C., 1998, A Benthic Annular Flume for in Situ Measurement of
691 Suspension Feeding/Biodeposition Rates and Erosion Potential of Intertidal Cohesive Sediments: Estuarine,
692 Coastal and Shelf Science, v. 46, p. 27-38.
693 Williamson, H.J., 1991, Tidal Transport of Mud/Sand Mixtures - A Literature Review: Sediment Distributions Report, v. SR
694 286.
695 Winterwerp, J.C., and Van Kesteren, W.G.M., 2004, Introduction to the Physics of Cohesive Sediment in the Marine
696 Environment, Amsterdam, Elsevier, p. 466.
697 Wright, J., Colling, A., and Park, D., 1999, Waves, Tides and Shallow-Water Processes: Oxford, U.K., Butterworth
698 Heinemann, p. 227.
699 Young, R.N., and Southard, J.B., 1978, Erosion of Fine-Grained Marine Sediments: Sea-Floor and Laboratory Experiments,
700 Geological Society of America, Bulletin, v. 89, p. 663-672.
701 Zajac, R., Whitlatch, R., and Thrush, S., 1998, Recolonization and Succession in Soft-Sediment Infaunal Communities: the
702 Spatial Scale of Controlling Factors: Hydrobiologia, v. 375-376.

FIGURE CAPTIONS

Fig. 1: Grain-size distribution of the extracted sand (D_{50}, 235 µm) and silt (D_{50}, 55 µm) components.

Fig. 2: Schematic and photograph of the annular flume (Aquatic Research Centre, University of Waikato, New Zealand).

Fig. 3: A) Photos showing the results of one "low" (118 g/m²) and one "high" (941 g/m²) silt concentration run from the layering experiments and B) one "low" (120 g/m³) and one "high" (1200 g/m³) run of the mixing experiments.

Fig. 4: Time series of the suspended-sediment concentrations (mg/l). A) Silt erosion during the layering experiment that occurred following 11 incremental changes in flume flow speed up to 0.30 m/s. Note that the flow speed was increased from 0.20 to 0.25 m/s in one increment, all other increments were 0.025 m/s. The size colored lines correspond to pure sand, "low" 29, 118, and 235 g/m², and "high" silt (353, 471, and 941 g/m²) concentrations. The initiation of sand erosion and silt erosion is highlighted by dashed black lines. B) Silt erosion during the mixing experiment that occurred following 11 incremental changes in flow speed up to 0.30 m/s. The initiation of sand erosion is highlighted by a dashed black line. Note that the flow speed was increased from 0.20 to 0.25 m/s.

Fig. 5: Mean erosion rates (mg/m²/s) against bed shear stress (N/m²) calculated as the initial slope of the hyperbolic-tangent fit to the observations in Figure 4. A) Layering experiments (Experiment 1) B) Mixing experiments (Experiment 2). The erosion behavior of pure silt and sand to silt is compared to layered sediment beds. Note that the flow speed was increased from 20 to 25 cm/s. For further explanations, see text.

Fig. 6: Conceptual model of the stabilization process. Large, white particles represent sand, and small, black particles correspond to silt. (A, B) silt deposited on top of a sand bed. A) The sediment bed was not stabilized, allowing inflow into the sand bed due to "undersaturated" pore space. B) Stable case: the pore space was filled by silt, causing a blocked inflow "blocked layer". (C, D) silt mixed into a sand bed. C) The sediment bed was not stabilized, allowing inflow into the sand bed due to "undersaturated" pore space. D) Stable case: the pore space was filled by silt throughout the whole sediment bed, causing a blocked inflow "blocked layer".

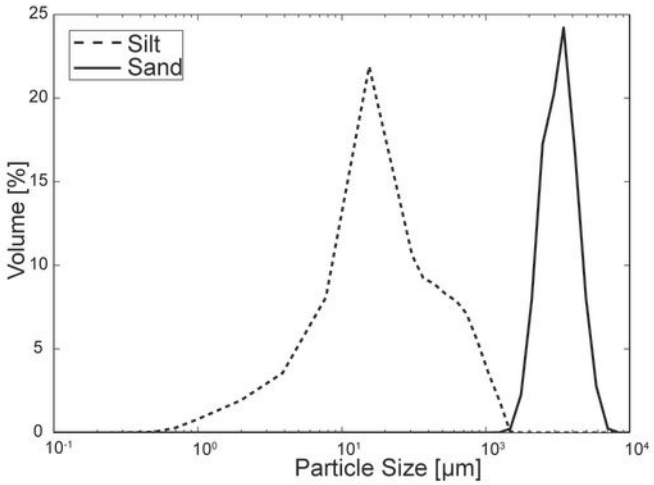
Silt
Sand
Volume [%]
Particle Size [µm]
25
20
15
10
5
0
10-1
100
101
103
104

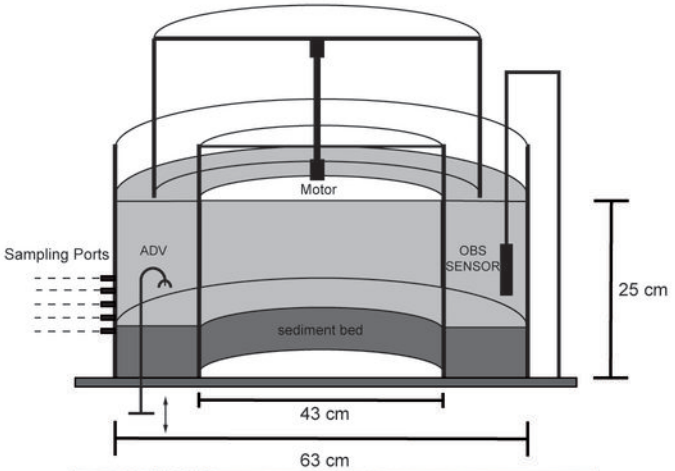
Motor
Sampling Ports
ADV
OBS
SENSOR
25 cm
sediment bed
43 cm
63 cm

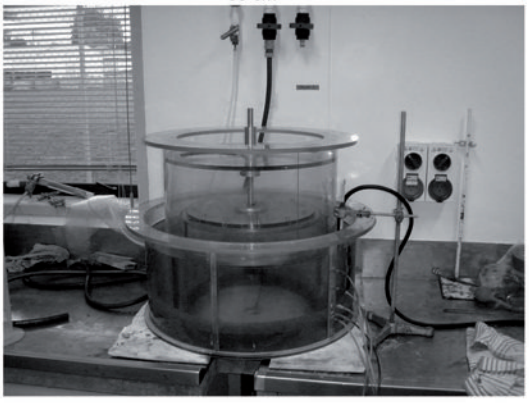

A) Layering experiments

1A) Low silt (118 g/m^2) concentration run - Initial stage

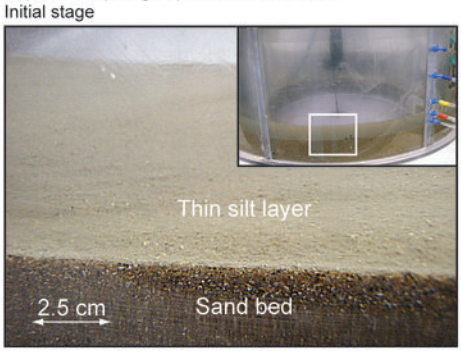

1B) Low silt (118 g/m^2) concentration - Final stage (0.30 m s^{-1})

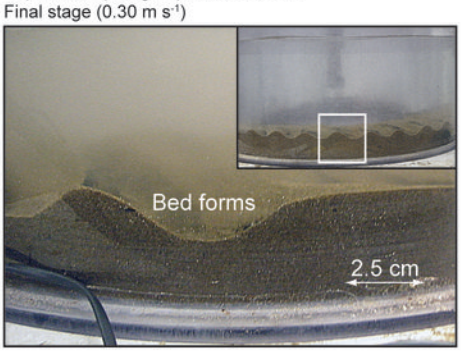

2A) High silt (941 g/m^2) concentration run - Initial stage

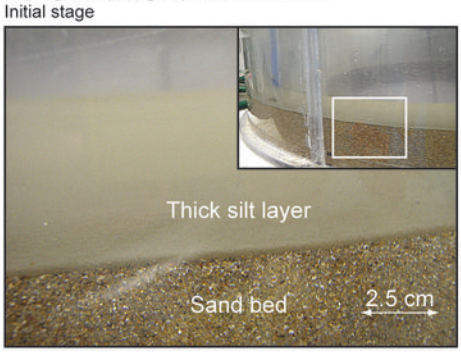

2B) High silt (941 g/m^2) concentration run - Final stage (0.30 m s^{-1})

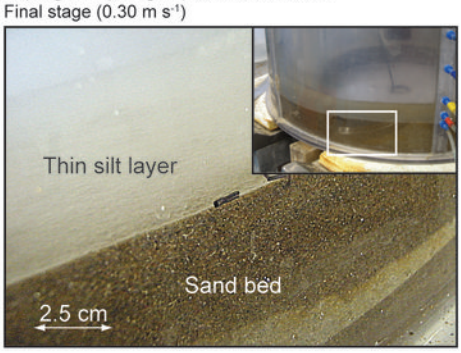

B) Mixing experiments

3A) Low silt (120 g/m^3) concentration run - Initial stage

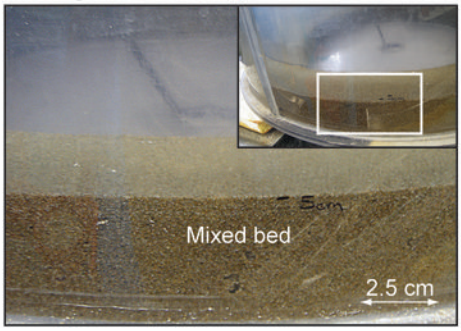

3B) Low silt (120 g/m^3) concentration run - Final stage (0.30 m s^{-1})

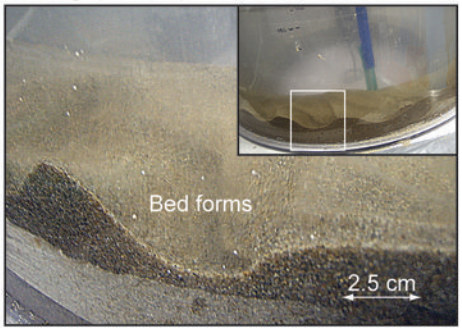

4A) High silt (1200 g/m^3) concentration run - Initial stage

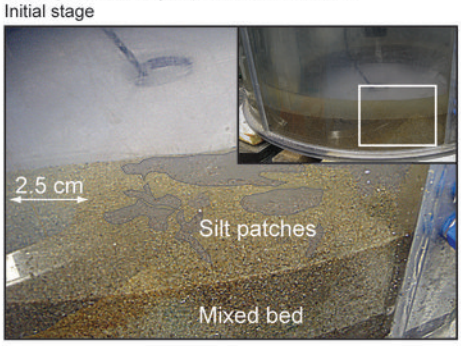

4B) High silt (1200 g/m^3) concentration run - Final stage (0.30 m s^{-1})

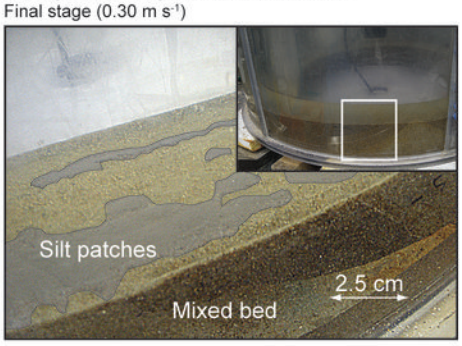

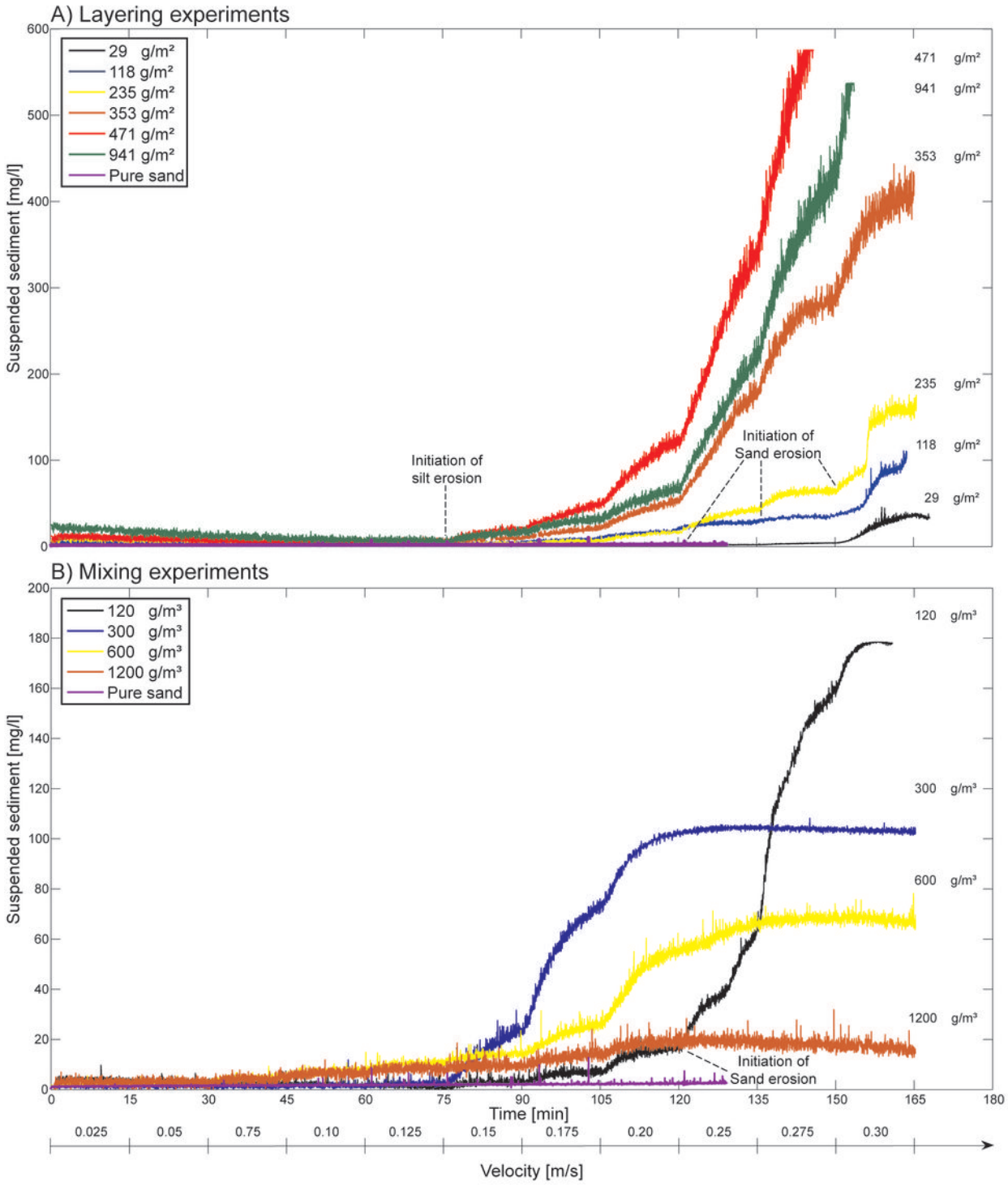
A) Layering experiments
29 g/m²
118 g/m²
235 g/m²
353 g/m²
471 g/m²
941 g/m²
Pure sand
Suspended sediment [mg/l]
Initiation of silt erosion
Initiation of Sand erosion
B) Mixing experiments
120 g/m³
300 g/m³
600 g/m³
1200 g/m³
Pure sand
Suspended sediment [mg/l]
Initiation of Sand erosion
Time [min]
Velocity [m/s]
0.025
0.05
0.75
0.10
0.125
0.15
0.175
0.20
0.25
0.275
0.30

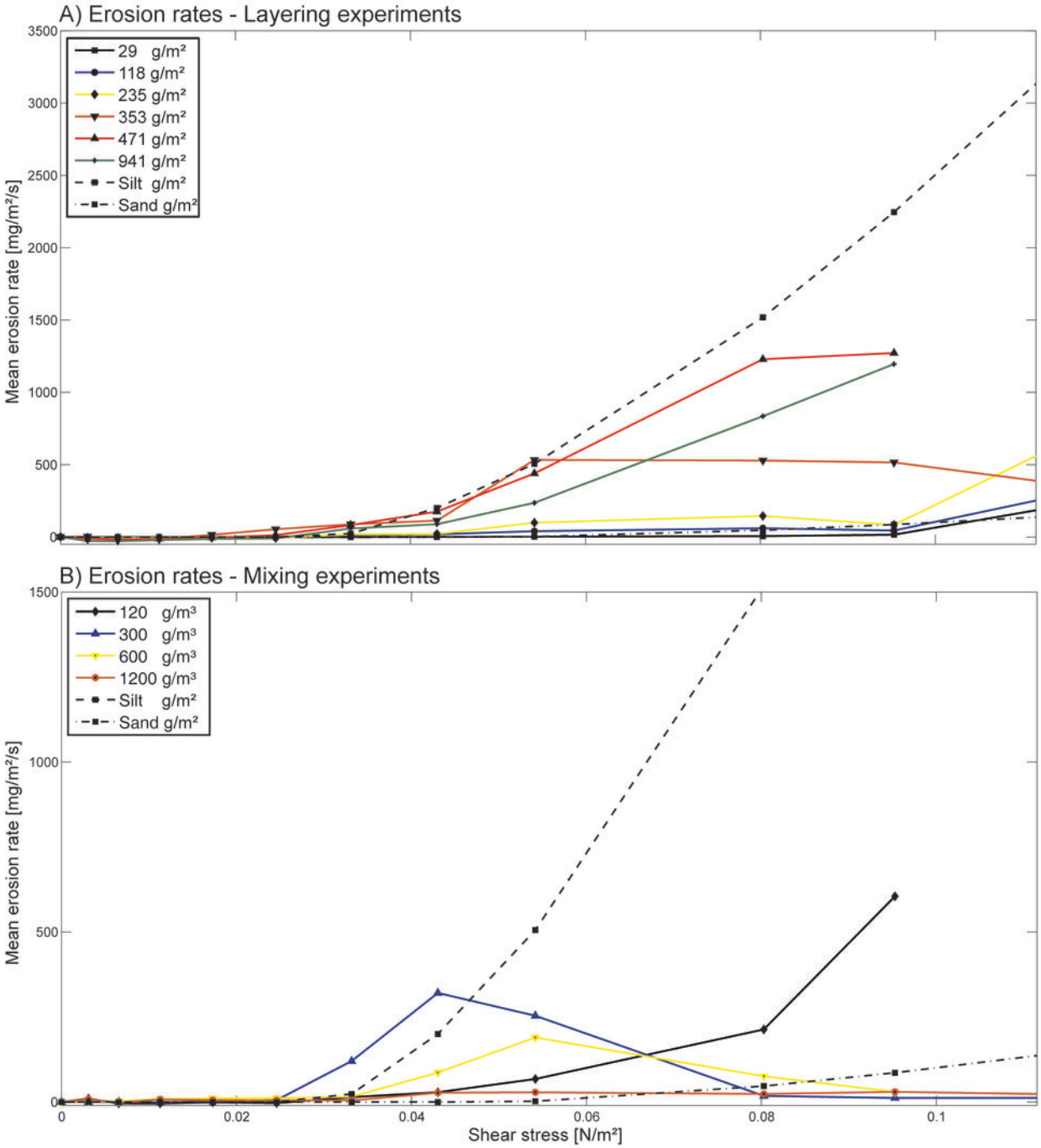
A) Erosion rates - Layering experiments
29 g/m²
118 g/m²
235 g/m²
353 g/m²
471 g/m²
941 g/m²
Silt g/m²
Sand g/m²
Mean erosion rate [mg/m²/s]
3500
3000
2500
2000
1500
1000
500
0
B) Erosion rates - Mixing experiments
120 g/m³
300 g/m³
600 g/m³
1200 g/m³
Silt g/m²
Sand g/m²
Mean erosion rate [mg/m²/s]
1500
1000
500
0
0
0.02
0.04
0.06
0.08
0.1
Shear stress [N/m²]

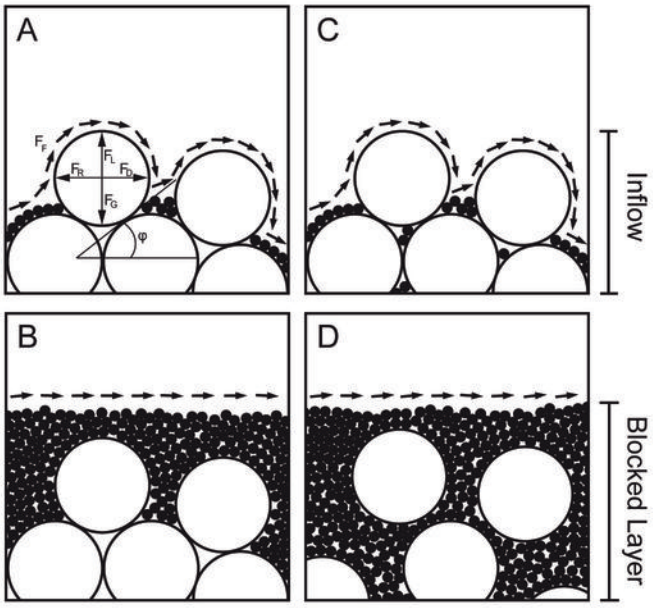
A
C
B
D
F_F
F_L
F_R
F_D
F_G
φ
Inflow
Blocked Layer

Table 1: Overview of experiments

	Duration [h:min]	Sediment type [mm]		Silt concentration	Velocity range [m/s]
"1.The Layering Experiment"					
Phase I deposition	04:00	Sand 0.03	Silt 0.0055	29, 118, 235, 353, 471, 941g/m²	0.025
Phase II-erosion	02:45	Sand 0.03	Silt 0.0055	29, 118, 235, 353, 471, 941g/m²	0.025-0.300
"2. The Mixing Experiment"					
Phase I consolidation	12:00	Sand 0.03	Silt 0.0055	120, 300, 600, 1200 g/m³	0.000
Phase II-erosion	02:45	Sand 0.03	Silt 0.0055	120, 300, 600, 1200 g/m³	0.025-0.300

Table 2: Overview of the sediment behavior derived from flume experiments

"1. The Layering Experiments"

Silt concentration [g/m²]	Critical velocity for silt [m/s]	Critical velocity for sand [m/s]	Maximal erosion rate [mg/m²/s]	Hydraulic conductivity [m/s]
0.0	0.15	0.15	not measured	0.00064
0.3	0.15	0.15	185	0.00063
1.0	0.15	0.2	252	0.00064
2.0	0.15	0.25	561	0.00061
3.5	0.15	> 0.30	533	0.00058
5.0	0.15	> 0.30	1272	0.00056
9.5	0.15	> 0.30	1196	0.00045

"2. The Mixing Experiments"

Silt concentration [g/m³]	Critical velocity for silt [m/s]	Critical velocity for sand [m/s]	Maximal erosion rate [mg/m²/s]	Hydraulic conductivity [m/s]
0	0.15	0.15	not measured	0.00064
120	0.15	0.15	605	0.00062
300	0.15	> 0.30	321	0.00049
600	0.15	> 0.30	190	0.00034
1200	0.15	> 0.30	30	0.00019